Downloaded from http://rspa.royalsocietypublishing.org/ on March 31, 2016

PROCEEDINGS OF THE ROYAL SOCIETY A

rspa.royalsocietypublishing.org

Research

Cite this article: Milewski PA, Vanden-Broeck J-M, Wang Z. 2013 Steady dark solitary flexural gravity waves. Proc R Soc A 469: 20120485. http://dx.doi.org/10.1098/rspa.2012.0485

Received: 18 August 2012
Accepted: 1 November 2012

Subject Areas:
applied mathematics

Keywords:
dark solitary waves, water waves, flexural gravity waves

Author for correspondence:
Paul A. Milewski
e-mail: p.a.milewski@bath.ac.uk

Royal Society Publishing
Informing the science of the future

Steady dark solitary flexural gravity waves

Paul A. Milewski[1], Jean-Marc Vanden-Broeck[2] and Zhan Wang[3]

[1]Department of Mathematical Sciences, University of Bath, Bath BA2 7AY, UK
[2]Department of Mathematics, University College London, London WC1E 6BT, UK
[3]Department of Mathematics, University of Wisconsin, Madison, WI 53706, USA

The nonlinear Schrödinger (NLS) equation describes the modulational limit of many surface water wave problems. Dark solitary waves of the NLS equation asymptote to a constant in the far field and have a localized decrease to zero amplitude at the origin, corresponding to water wave solutions that asymptote to a uniform periodic Stokes wave in the far field and decreasing oscillations near the origin. It is natural to ask whether these dark solitary waves can be found in the irrotational Euler equations. In this paper, we find such solutions in the context of flexural-gravity waves, which are often used as a model for waves in ice-covered water. This is a situation in which the NLS equation predicts *steadily* travelling dark solitons. The solution branches of dark solitons are continued, and one branch leads to fully localized solutions at large amplitudes.

1. Introduction

Solitary waves play a central role in free surface and interfacial flows. In the water wave problem, the existence of various types of solitary waves is often hinted at by model equations (Korteweg–de Vries, Kadomtsev–Petviasvilli, nonlinear Schrödinger, and so on) or local bifurcation analysis. Fully nonlinear waves can then be sought through numerical means or proved via analytical means. In particular, the (1+1)-dimensional nonlinear Schrödinger (NLS) equation that governs the modulation of quasi-monochromatic waves has

© 2012 The Authors. Published by the Royal Society under the terms of the Creative Commons Attribution License http://creativecommons.org/licenses/by/3.0/, which permits unrestricted use, provided the original author and source are credited.

Downloaded from http://rspa.royalsocietypublishing.org/ on March 31, 2016

families of solutions, among which, bright or dark solitons depending on the coefficients of the equation (corresponding to the focusing or defocusing cases, respectively) [1,2]. Bright solitons of NLS can be used to construct fully nonlinear capillary-gravity wave-packet solitary waves [3].

In this paper, we seek to find the counterpart of dark solitons of NLS in the Euler equations. In order to do so, we consider the problem of flexural-gravity waves in infinite depth: the propagation of waves in a semi-infinite fluid bounded above by a solid sheet that responds to flexural (bending) forces only. This is a commonly used model for waves under floating ice [4]. Dark solitary wave solutions are sought in this context because: (i) the linear dispersion relation has a minimum of phase speed at finite wavenumber, which means that at that wavenumber, phase and group speed are equal, thus allowing for steadily travelling small amplitude nonlinear wave-packets and (ii) in the case of deep enough water, the coefficients of the NLS equation for this wavenumber correspond to the *defocusing* case, which is the case for which dark solitary waves are expected. Dark solitons derive their name from nonlinear optics where they have been studied and observed experimentally [5,6] and correspond to a relatively localized *decrease to zero* in intensity of the wave-field. Whereas in nonlinear optics, the NLS equation is usually used *ab initio*, in fluid mechanics it represents an asymptotic model whose predictions need to be verified against solutions of the full potential flow equations. In this paper, we compute dark soliton-like structures in the full potential flow equations and follow the solution branch to amplitudes beyond those described by the NLS equation. To our knowledge, this is the first computation of travelling dark solitons in free-surface fluid flows.

The modulational dynamics of weakly nonlinear surface wave-packets in one space dimension can be described by the NLS equation

$$\mathrm{i}A_T + \lambda A_{XX} = \mu |A|^2 A, \tag{1.1}$$

where A is the complex envelope of a carrier wave with wavenumber k^* and $\mu(k^*)$; $\lambda(k^*)$ are real coefficients. The primitive free surface variable $\zeta(x,t)$ is given by

$$\zeta \sim \epsilon[A(X,T)\,\mathrm{e}^{\mathrm{i}(k^*x-\omega(k^*)t} + \bar{A}(X,T)\,\mathrm{e}^{-\mathrm{i}(k^*x-\omega(k^*)t}] + O(\epsilon^2).$$

Here, ϵ is a non-dimensional small amplitude, $T=\epsilon^2 t$, $X=\epsilon(x-c_g(k^*)t)$, $\omega(k)$ is the dispersion relation of the original system and $c_g(k)\equiv\omega'(k)$ is the group velocity. If the product of the coefficients $\lambda\mu<0$, the equation is of the focusing type, and there exist travelling solitary wave solutions corresponding to localized wavepackets. If the product of the coefficients $\lambda\mu>0$, the equation is of the defocusing type, and there are travelling 'dark solitons' that are periodic wavetrains with a localized decrease in amplitude (and a shift of π in phase) [2].

In fluid problems, travelling wave solutions to the NLS equation correspond, in general, to *unsteady* solutions in the primitive variables because the envelope travels at speeds close to the group velocity whereas the carrier wavecrests travels at the phase velocity. One important special case is when these two velocities are equal, which occurs at an extremum of the phase speed $c(k)\equiv\omega(k)/k$. In this case, the NLS solutions describe approximate steadily *travelling solutions* in the *primitive* variables [3,7] and exact travelling solutions may be sought. For the bright solitons of the focusing NLS equation, under these conditions, and in the setting of gravity-capillary waves, the resulting solitary water wave can be found in the primitive potential flow equations [8]. The condition of group and phase speed being equal renders the computation tractable since by seeking travelling wave solutions of the primitive equations, the dimensionality of the problem is reduced by one. In this paper, we show that *dark* soliton solutions can also be found in the potential flow equations. At larger amplitudes, we shall see that the dark solitary wave branch yields solutions that appear to consist of two bright wavepacket waves with small non-decaying periodic tails.

2. Formulation

Consider the problem of surface waves on a semi-infinite ideal fluid in two dimensions bounded above by a flexible elastic sheet. The two competing restoring forces are gravity and the flexural

Downloaded from http://rspa.royalsocietypublishing.org/ on March 31, 2016

elasticity of the sheet. The irrotational Euler equations with the fully nonlinear kinematic and dynamic boundary conditions are used for the fluid, and the simplest Kirchoff–Love nonlinear elasticity model appropriate for thin flexible sheets is used for the solid as in [9,10]. This elasticity model yields a restoring force in the form of a pressure jump across the elastic sheet equal to

$$D\partial_x^2\kappa,$$

where D is the flexural rigidity of the sheet and κ is its curvature. Denoting the free surface by $y=\zeta(x,t)$ and the velocity potential by $\phi(x,y,t)$, the governing equations for the flow and the boundary conditions are given by

$$\Delta\phi=0 \quad \text{for } -\infty<y<\zeta(x,t), \tag{2.1}$$

$$\phi\to 0 \quad \text{as } y\to-\infty, \tag{2.2}$$

$$\zeta_t+\phi_x\zeta_x=\phi_y \quad \text{at } y=\zeta(x,t) \tag{2.3}$$

and

$$\phi_t=-\frac{1}{2}[\phi_x^2+\phi_y^2]-\zeta-\partial_{xx}\frac{\zeta_{xx}}{(1+\zeta_x^2)^{3/2}} \quad \text{at } y=\zeta(x,t). \tag{2.4}$$

These equations have been made dimensionless by choosing

$$\left(\frac{D}{\rho g}\right)^{1/4},\quad \left(\frac{D}{\rho g^5}\right)^{1/8},\quad \left(\frac{Dg^3}{\rho}\right)^{1/8},\quad (D\rho^3 g^3)^{1/8}$$

as the units of length, time, velocity and pressure, where ρ is the density of the fluid and g is the acceleration owing to gravity. Travelling solutions to the potential flow equations (2.1)–(2.4) with wave speed c can be found by assuming that all functions in the original variables depend on $x-ct$, thus replacing time derivatives with $-c\partial_x$.

In order to handle the unknown free surface, we reformulate this system using a conformal map from the physical domain to the lower-half plane with horizontal and vertical coordinates denoted by ξ and η, respectively. The map can be found by solving the harmonic boundary value problem

$$\begin{aligned} y_{\xi\xi}+y_{\eta\eta}&=0 \quad \text{for } -\infty<\eta<0,\\ y&=Y(\xi) \quad \text{at } \eta=0,\\ y&\sim\eta \quad \text{as } \eta\to-\infty, \end{aligned}$$

where $Y(\xi,t)=\zeta(x(\xi,0))$. The harmonic conjugate variable $x(\xi,\eta)$ is defined through the Cauchy–Riemann relations for the complex function $z(\xi,\eta)=x(\xi,\eta)+\mathrm{i}y(\xi,\eta)$. In the transformed plane, the velocity potential $\phi(\xi,\eta)\triangleq\phi(x(\xi,\eta),y(\xi,\eta))$ and its harmonic conjugate $\psi(\xi,\eta)$ also satisfy Laplace's equation.

Under this transformation, the kinematic boundary condition becomes $\Psi=cY$, the conjugate variable relation yields

$$X_\xi=1-\mathscr{H}[Y_\xi], \tag{2.5}$$

and the dynamic boundary condition becomes

$$\frac{c^2}{2}\left(\frac{1}{J}-1\right)+Y+\frac{M}{X_\xi^3 J^{7/2}}=0, \tag{2.6}$$

where $J=X_\xi^2+Y_\xi^2$, $\mathscr{H}$ is the Hilbert transform and the bending term M is a lengthy function given in [11]. These equations complete an integro-differential system for the free surface displacement Y. They are equivalent to that obtained in [10] by using a conformal map on a steady solution under the action of a mean flow opposite c.

Downloaded from http://rspa.royalsocietypublishing.org/ on March 31, 2016

Linearizing (2.1)–(2.4) and assuming monochromatic waves $\zeta = A\,\mathrm{e}^{\mathrm{i}(kx-\omega t)}$ and $\phi = B\,\mathrm{e}^{|k|y}\,\mathrm{e}^{\mathrm{i}(kx-\omega t)}$, one obtains the dispersion relation

$$\omega^2 = |k|(1+k^4) \quad \text{or} \quad c^2 = \left(\frac{1}{|k|} + |k|^3\right), \tag{2.7}$$

which has a phase speed minimum with

$$k^* = (\tfrac{1}{3})^{1/4} \approx 0.7598, \quad c^* = \sqrt{3^{1/4} + 3^{-3/4}} \approx 1.3247.$$

The equation governing modulations of a monochromatic wave is derived by substituting

$$\begin{pmatrix}\zeta\\ \phi\end{pmatrix} \sim \epsilon \begin{pmatrix}A(X,T)\\ B(X,T)\,\mathrm{e}^{|k|y}\end{pmatrix} \mathrm{e}^{\mathrm{i}(kx-\omega t)} + \text{c.c.} + \epsilon^2 \begin{pmatrix}\zeta_1\\ \phi_1\end{pmatrix} + \epsilon^3 \begin{pmatrix}\zeta_2\\ \phi_2\end{pmatrix} + \cdots \tag{2.8}$$

into (2.1)–(2.4), and ensuring that the series is well ordered for $t = O(\epsilon^{-2})$. The steps are standard and we state the results for the minimum speed carrier wave k^* only. Then, A satisfies (1.1), $B = -\mathrm{i}c^*A$, and

$$\lambda = \frac{3^{7/8}}{2}, \quad \mu = \frac{79}{88}3^{-9/8}.$$

Because $\lambda\mu > 0$, there is a family of dark solitary waves given by

$$A = a\tanh(qX)\,\mathrm{e}^{-\mathrm{i}\Omega T}, \quad q = \left(\frac{\mu}{2\lambda}\right)^{1/2} a, \quad \Omega = \mu a^2. \tag{2.9}$$

In the original fluid equations, these solutions asymptote to the first-order Stokes' wave solution in the far field. Stokes-like waves with A constant have the same amplitude-dependent frequency $\Omega(a)$. The Stokes and dark solitary waves have $c > c^*$ with approximate speed–amplitude dependence in the primitive variables given by

$$c - c^* \sim \frac{\mu}{4k^*}|\zeta_{\max}|^2.$$

These results will be compared below with the numerically computed solutions to the full potential flow system. We restrict ourselves in this paper to dark solitary waves with zero amplitude at the origin and with a phase-shift of π in the carrier wave between $\pm\infty$, corresponding, in the NLS case, to (2.9). In addition to these, the NLS equation supports 'grey' solitary waves, depending on an additional parameter K

$$A = \frac{a}{\sqrt{q^2+K^2}}[q\tanh(qX) - \mathrm{i}K]\,\mathrm{e}^{\mathrm{i}(KX-\Omega T)}$$

and

$$q^2 = \left(\frac{\mu}{2\lambda}\right)a^2 - K^2, \quad \Omega = \mu a^2 + \lambda K^2.$$

For $0 < K \leq (\mu/2\lambda)^{1/2}a$, these solutions are also asymptotic to Stokes' waves at infinity, but have a non-zero minimum amplitude of $(2\lambda/\mu)^{1/2}K$ at the origin and a phase shift $2\tan^{-1}(q/K) < \pi$. We believe that there is no *a priori* reason that such solutions cannot be translated into steadily travelling solutions of the potential flow equations, but their numerical computation appears more delicate. Solutions of this type will therefore be considered elsewhere.

3. Results

Two new branches of solutions to the full travelling-wave potential equations (2.5)–(2.6) are computed on a large periodic domain using a Fourier approximation. The resulting algebraic equations for the Fourier coefficients are solved using Newton's method, and once a solution on a branch is found, solutions along this branch are computed through continuation methods. It is somewhat delicate to find the initial dark solitary wave solutions because there are other solutions (such as constant amplitude nonlinear periodic Stokes waves) with the same carrier

Downloaded from http://rspa.royalsocietypublishing.org/ on March 31, 2016

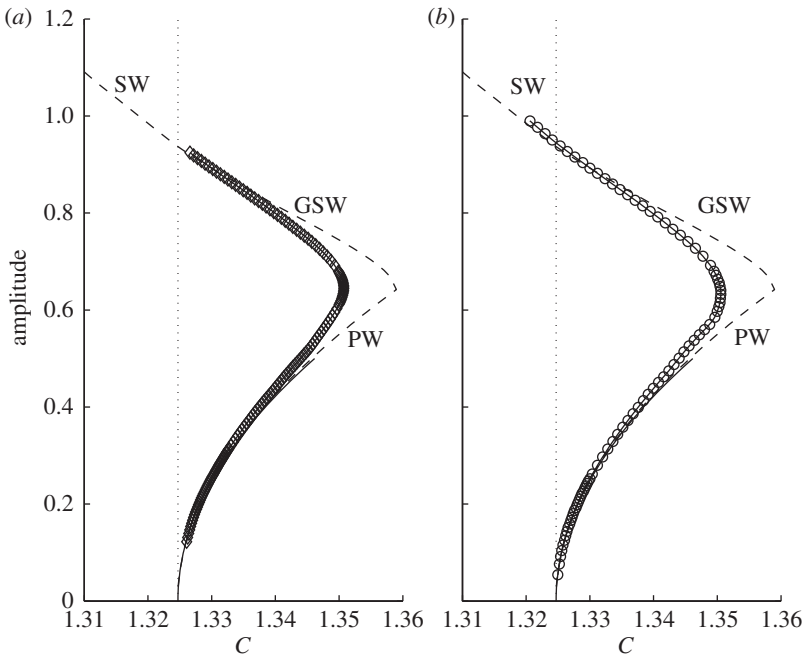

Figure 1. Speed–amplitude solution curves for travelling wave branches near the minimum linear speed c^* (which is shown by the vertical line). The dashed curves labelled SW, GSW and PW correspond to, respectively, the bright solitary, generalized solitary and periodic travelling waves discussed in [11]. There are two dark solitary wave branches shown with diamonds and circles corresponding, at small amplitudes, to the two cases of (3.1). The branch of waves with a minimum at $x = 0$ at small amplitude (see figure 2) is shown on (*a*) (diamonds). The branch of waves with a maximum at $x = 0$ at small amplitude (see figure 3) is shown on (*b*) (circles). This latter solution branch can be extended to $c < c^*$, where it is no longer a dark soliton, but a solitary wave. In both graphs, the solid line is the speed–amplitude curve predicted by the NLS equation. The amplitude parameter in all cases is $\frac{1}{2}[\max(Y) - \min(Y)]$.

period and nonlinear speed. In order to find an initial branch of non-trivial dark solitary solutions, we fix $c < c^*$ and add a localized 'forcing' $F(x - ct)$ (physically corresponding to a pressure force on the free surface) to (2.5)–(2.6). This forced branch is then continued by increasing c to values $c > c^*$, where the solutions are no longer localized near the forcing, and have periodic 'tails'. If one then removes the forcing gradually, one obtains free finite-amplitude solutions (i.e. the tails alone, without the localized disturbance of the forced solution). In most cases, the method we just described yields uniform periodic Stokes waves. Dark solitary waves are found by choosing judiciously the computational domain length L. For $c \approx c^*$, the tails described above are the carrier wave that we wish to modulate into a dark solitary wave. This carrier wave has a period close to $2\pi/k^*$. Because dark solitary waves (2.9) add a phase shift of π to the carrier, we chose a domain $L \approx (2n + 1)\pi/k^*$ for a relatively large n. This forces the solution to have the requisite phase shift and avoids the purely periodic Stokes wave. All solutions were assumed to be even about $x = 0$, and this symmetry centres the dark solitary wave there. In most examples presented, $L = 368.4$ and $n = 44$. In the computations shown typically 1024 Fourier modes provide accurate solutions although we performed computations at different resolutions to confirm convergence. The convergence criterion was that the residual, measured in the l_1-norm, was less than 10^{-10}.

There are two families of even solutions that can be sought. Because the NLS solution (2.9) is odd about $x = 0$, the carrier wave also has to be odd, of the form $\pm 2\sin(k^*(x - c_p t))$, resulting in two free surface profiles at small amplitude:

$$\zeta \sim \pm 2\epsilon a \tanh\left(\epsilon a \left(\frac{\mu}{2\lambda}\right)^{1/2} (x - c_g t)\right) \sin\left(k(x - (c_p + \mu(\epsilon a)^2)t)\right). \tag{3.1}$$

Downloaded from http://rspa.royalsocietypublishing.org/ on March 31, 2016

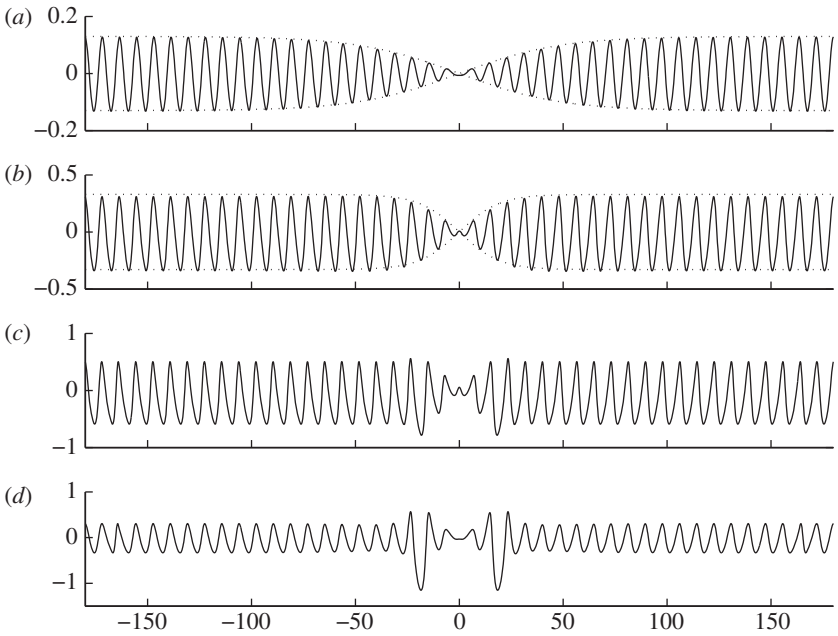

Figure 2. Travelling dark wave solitary wave solutions corresponding to the positive sign branch in (3.1). From (*a–d*), one moves along the branch increasing the amplitude parameter from solutions whose envelope is well described by the dark soliton of NLS (dashed line) to a solution that resembles pairs of bright solitary waves with non-decaying periodic tails.

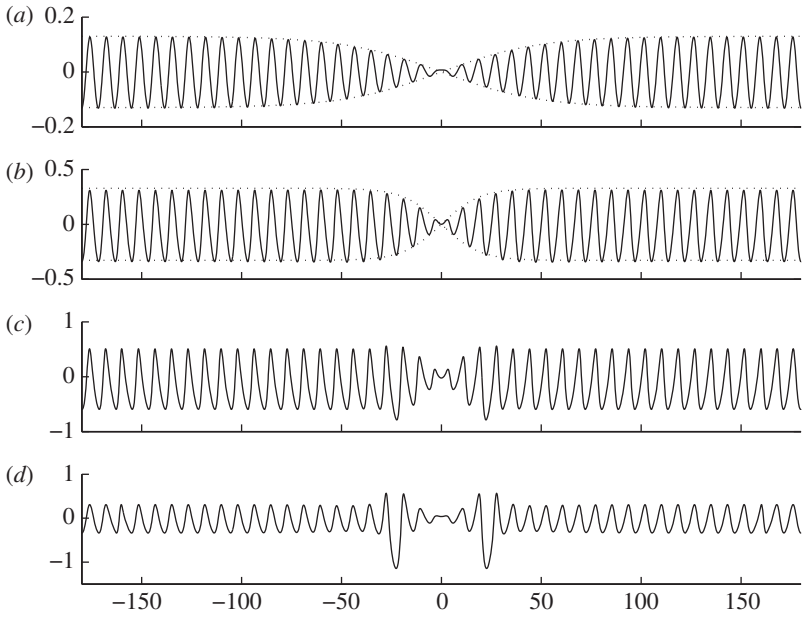

Figure 3. Travelling dark wave solitary wave solutions corresponding to the negative sign branch in (3.1). From (*a–d*), one moves along the branch increasing the amplitude parameter from solutions whose envelope is well described by the dark soliton of NLS (dashed line) to a solution that resembles pairs of bright solitary waves with non-decaying periodic tails.

The positive sign corresponds to a wave with a minimum at $x = 0$, whereas the negative sign wave has a corresponding maximum. This distinction seems to be valid only at very small amplitude.

Downloaded from http://rspa.royalsocietypublishing.org/ on March 31, 2016

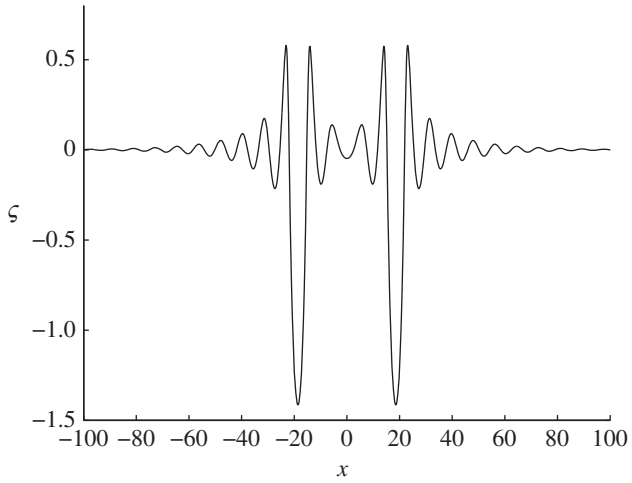

Figure 4. Localized solution on the dark solitary wave branch. The solution was computed on the same domain as in figure 3 but is shown on a smaller domain.

In figure 1, we show the bifurcation diagram for these two branches of dark solitary waves, together with the branches of bright solitary (localized wave packet solitary waves), generalized solitary waves (wavepacket solitary with finite amplitude far field oscillations) and periodic waves found previously in [11]. Note that, even though small amplitude wave packet solitary waves are not allowed by the defocusing NLS equation in this situation, they do occur at large amplitudes. The two new branches of dark solitary waves compare well with the predictions from the NLS equation for small amplitude. At larger amplitude, the branches of solution follow closely those of generalized solitary waves. In figures 2 and 3, sample profiles along the dark solitary wave branches corresponding to the two cases in (3.1) are shown. Clearly, as the amplitude increases, the solution transitions from a hyperbolic tangent-like dark soliton to pairs of large amplitude bright solitons with non-decaying periodic tails akin to those found in [11]. The principal difference at larger amplitudes between the solution of figures 2 and 3 is the separation distance between the two largest troughs. Solution curves in figure 1 are shown up to the points where we feel confident that the solutions are well resolved (by changing domain size and resolution). The continuation of the branches past these points was delicate with slow convergence of Newton iterations and high sensitivity on domain size and resolution. One of the branches could be continued to the region $c < c^*$ and the solution, as seen in figure 4 becomes localized on two bright solitary waves.

4. Conclusions

Dark solitary wave solutions, predicted by the NLS equation, were successfully computed in the primitive irrotational Euler equations for water waves with flexural-gravity boundary conditions. The NLS solutions approximate these waves well for small amplitude, but at larger amplitudes we find that the branches become a pair of bright solitary or a pair of bright generalized solitary waves. While the infinite extent of these dark solitons may preclude their observation, the existence of these waves point to the possibility of 'wave defects' in more realistic situations where the phase of the carrier wave jumps by $\pm\pi$. There are other possible free surface fluid systems with travelling wave dark solitons worth investigating, most notably the interfacial problem between two immiscible fluids of different densities, under the action of both gravity and surface tension forces. In this case, if the densities are close, the defocusing NLS equation arises out of a minimum of the phase speed [12] and we expect, similarly, the full equations to have dark solitary waves.

Downloaded from http://rspa.royalsocietypublishing.org/ on March 31, 2016

More generally, these results for travelling waves are a good indication that unsteady dark solitary waves could also, in principle, be found in the primitive potential flow equations, for example in deep water gravity waves. Theoretical arguments for this are given in [13].

This work was supported by EPSRC, under grant nos. GR/S47786/01, EP/J019569/1 and EP/J019321/1, and by the Division of Mathematical Sciences at the National Science Foundation, under grant no. DMS-0908077 and by a Royal Society Wolfson award.

References

1. Ablowitz MJ, Segur H. 1979 On the evolution of packets of water waves. *J. Fluid. Mech.* **92**, 691–715. (doi:10.1017/S0022112079000835)
2. Peregrine DH. 1983 Water waves, nonlinear Schrödinger equations and their solutions. *J. Fluid Mech.* **536**, 99–105. (doi:10.1017/S0334270000003891)
3. Akylas TR. 1993 Envelope solitons with stationary crests. *Phys. Fluids A* **5**, 789–791. (doi:10.1063/1.858626)
4. Squire VA, Hosking RJ, Kerr AD, Langhorne PJ. 1996 *Moving loads on ice plates*. Solid Mechanics and its Applications. Dordrecht, the Netherlands: Kluwer.
5. Emplit P, Hamaide JP, Reynaud F, Froehly C, Barthelemy A. 1987 Picosecond steps and dark pulses through nonlinear single mode fibers. *Opt. Commun.* **62**, 374–379. (doi:10.1016/0030-4018(87)90003-4)
6. Weiner AM, Heritage JP, Hawkins RJ, Thurston RN, Kirschner EM, Leaird DE, Tomlinson WJ. 1988 Experimental observation of the fundamental dark soliton in optical fibers. *Phys. Rev. Lett.* **61**, 2445–2448. (doi:10.1103/PhysRevLett.61.2445)
7. Il'ichev AT. 2000 Solitary waves in media with dispersion and dissipation (a review). *Fluid Dynam.* **35**, 157–176. (doi:10.1007/BF02831423)
8. Vanden-Broeck J-M, Dias F. 1992 Gravity-capillary solitary waves in water of infinite depth and related free-surface flows. *J. Austral. Math. Soc. Ser. B* **25**, 16–43. (doi:10.1017/S0022112092000193)
9. Forbes LK. 1986 Surface waves of large amplitude beneath an elastic sheet. I. High-order series solution. *J. Fluid Mech.* **169**, 409–428. (doi:10.1017/S0022112086000708)
10. Parau E, Dias F. 2002 Nonlinear effects in the response of a floating ice plate to a moving load. *J. Fluid Mech.* **460**, 281–305. (doi:10.1017/S0022112002008236)
11. Milewski PA, Vanden-Broeck J-M, Wang Z. 2011 Hydroelastic solitary waves in deep water. *J. Fluid Mech.* **679**, 628–640. (doi:10.1017/jfm.2011.163)
12. Laget O, Dias F. 1997 Numerical computation of capillary-gravity interfacial solitary waves. *J. Fluid Mech.* **349**, 221–251. (doi:10.1017/S0022112097006861)
13. Bridges TJ, Donaldson NM. 2006 Secondary criticality of water waves. I. Defnition, bifurcation and solitary waves. *J. Fluid Mech.* **565**, 381–417. (doi:10.1017/S002211200600187X)